Constructing the Universe with Clusters of Galaxies, IAP 2000 meeting, Paris (France) July 2000
Florence Durret & Daniel Gerbal eds.

SUNYAEV-ZEL'DOVICH DETERMINED DISTANCES TO HIGH REDSHIFT GALAXY CLUSTERS

Erik D. Reese[1], John E. Carlstrom[1], Joseph J. Mohr[2], Marshall Joy[3], Laura Grego[4], William L. Holzapfel[5]

[1]*Department of Astronomy and Astrophysics, University of Chicago, 5640 S. Ellis Ave., Chicago, IL 60637*
[2]*Department of Astronomy, University of Illinois at Urbana-Champaign, 1002 West Green Street, Urbana, IL 61801*
[3]*Space Science Laboratory, SD50, NASA Marshall Space Flight Center, Huntsville, AL 35812*
[4]*Harvard-Smithsonian Center for Astrophysics, 60 Garden Street, Cambridge, MA 02138*
[5]*Department of Physics, University of California, Berkeley, Berkeley, CA 94720*

We present preliminary results from a maximum likelihood joint analysis of 30 GHz interferometric Sunyaev-Zel'dovich Effect (SZE) and X-ray observations for a sample of 14 high redshift ($0.14 \leq z \leq 0.78$) clusters of galaxies. From the joint SZE and X-ray analysis we determine the distances to the 14 galaxy clusters. These distances imply a Hubble parameter of 63^{+4+19}_{-4-19} km s^{-1} Mpc^{-1} for a $\Omega_M = 0.3$ and $\Omega_\Lambda = 0.7$ cosmology, where the uncertanties are statistical followed by systematic at 68% confidence. The implied Hubble constant is 59 km s^{-1} Mpc^{-1} for an open $\Omega_M = 0.3$ universe and 56 km s^{-1} Mpc^{-1} for a flat $\Omega_M = 1$ cosmology. We briefly discuss possible sources of systematic uncertainty and their controllable nature.

1 Introduction

Analysis of Sunyaev-Zel'dovich effect (SZE) and X-ray data from a cluster of galaxies provides information that can be used to determine the distance to the cluster, independent of the extragalactic distance ladder. The SZE[1,2] is the small (≤ 1 mK) distortion in the cosmic microwave background (CMB) spectrum caused by CMB photons inverse Compton scattering off the electrons in the hot (~ 10 keV) intracluster medium (ICM) trapped in the cluster potential well. This distortion appears as a decrement for frequencies ≤ 218 GHz ($\lambda \geq 1.4$ mm) and as an increment for frequencies ≥ 218 GHz. The SZE signal is proportional to the pressure integrated along the line of sight through the cluster, $\Delta T \sim \int n_e T_e d\ell$, where n_e is the electron density of the ICM and T_e is the electron temperature. The X-ray surface brigtness can be written as $S_x \sim \int n_e^2 \Lambda_{e\mathrm{H}} d\ell$ where $\Lambda_{e\mathrm{H}}$ is the X-ray cooling function, which depends on temperature and metallicity. The distance to the cluster can be determined by capitalizing on the different dependencies on density, n_e, with some assumptions about the geometry of the cluster. This is a direct distance based only on relatively simple cluster physics and not requiring any standard candles or rulers.

We present a joint maximum-likelihood fit to both interferometric SZE and X-ray data. This method takes advantage of the unique properties of interferometric SZE data, utilizing all the available image data on the ICM. We apply this method to a sample of 14 galaxly clusters with redshifts between 0.14 and 0.78 and use the distances to constrain the Hubble parameter, H_0. We describe the observations and data reduction in §2. We outline the analysis method and distance determinations in §3 and present our results and conclusions in §4. All uncertainties are at 68.3% confidence unless explicitly stated otherwise. We refer the reader to Reese et al. 2000 for a more detailed discussion of the data and the analysis method.

2 Observations and Reduction

2.1 Interferometric Sunyaev-Zel'dovich Effect Data

The extremely low systematics of interferometers and their two-dimensional imaging capability make them well suited to study the weak ($\leq$ 1 mK) SZE signal in galaxy clusters. Over the past several summers, we outfitted the Owens's Valley Radio Observatory (OVRO) and the Berkeley-Illinois-Maryland Association (BIMA) milimeter arrays with our own centimeter wave receivers (Carlstrom, Joy, & Grego 1996; Carlstrom et. al 1999). The receivers use cooled ($\sim$ 10 K) high electron mobility transistor (HEMT) amplifiers operating over 26-36 GHz with characteristic receiver temperatures of $T_{rx} \sim$ 11-20 K over the 28-30 GHz band used for the observations presented here. When interfaced with the BIMA and OVRO systems, these receivers obtain optimal system temperatures scaled to above the atmosphere of 34 K. Most telescopes are placed close together to probe the angular scales subtended by distant clusters ($\sim 1'$), but telescopes are always placed at longer baselines for simultaneous detection of point sources.

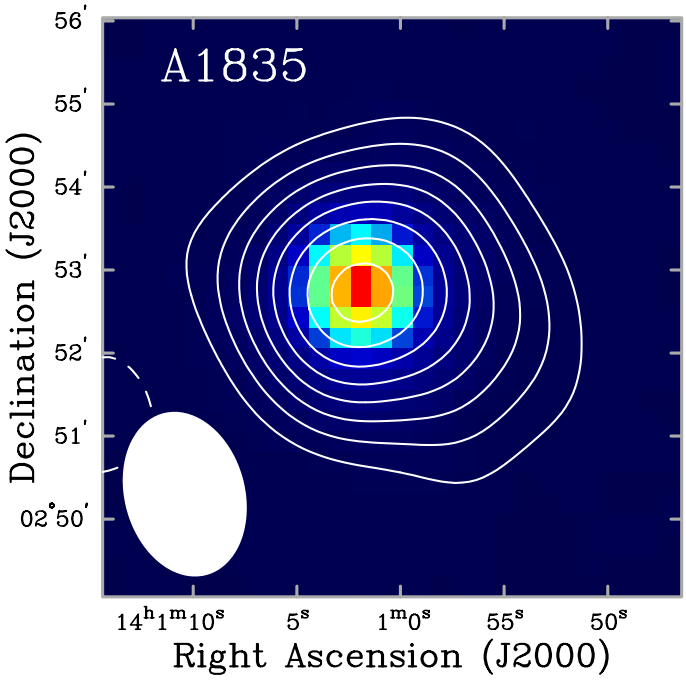

Figure 1: SZE (contour) and X-ray (image) overlay. The contours are the deconvolved (CLEANed) image from the naturaly weighted BIMA data of Abell 1835 using a 1000 λ half-power radius Gaussian to emphasize the brightness variations on cluster scales. The Rayleigh-Jeans brightness sensitivity rms is about 30 μK with a synthesized beam of 87×121 arcseconds FWHM (shown in lower left corner). The contours are multiples of twice the rms. The X-ray image is a Gaussian smoothed version of the PSPC raw counts image, which contains roughly 5000 source counts.

Figure 1 shows the deconvolved SZE image in contours overlaid on a color scale PSPC X-ray image of Abell 1835. To emphasize the angular scales of clusters, before deconvolving we apply a 1000 λ half-power radius Gaussian taper to the naturally weighted interferometric data giving a $87'' \times 121''$ synthesized beam and a rms of $\sim$ 213 μJy beam^{-1}, corresponding to a $\sim$ 30 μK Rayleigh-Jeans (RJ) brightness sensitivity. The SZE image contours are multiples of twice the rms noise level. We use the high resolution data ($\geq$ 2000 λ) to remove the two point sources in the field before deconvolving the cluster image; a $\sim$ 2.5 mJy point source located at the cluster center and a $\sim$ 1.0 mJy point source $\sim 50''$ from the cluster center. We stress that this SZE image demonstrates the data quality. The actual analysis is done in the Fourier plane, where the noise characteristics of the data and the spatial filtering of the interferometer are well

understood. The SZE and X-ray image overlay in Figure 1 show that the region of the cluster sampled by the interferometric SZE observations and the X-ray observations is similar.

2.2 X-ray Data

We use archival *Röntgen Satelite* (*ROSAT*) data, using data from both the Position Sensitive Proportional Counter (PSPC) and the High-Resolution Imager (HRI) available for each cluster. The data are reduced using the Snowden Extended Source Analysis Software[6,7] (ESAS) package. We use this software to generate a raw counts image, a noncosmic background image, and an exposeure map for the HRI (0.1-2.4 keV) data and for each of the Snowden bands R4-R7 (0.5-2.0 keV) for the PSPC data. We examine the light curve data of both instruments and excise periods of anomalously high counts rates (short-term enhancements) and periods of high scattered solar X-ray contamination. The Snowden software produces 512×512 pixel images with $14''.947$ pixels for the PSPC and $5''.0$ pixels for the HRI. For the PSPC, final images for all of the R4-R7 bands together are generated by adding raw counts images and background images, and constructing cluster-count-weighted averages for the exposure image and the point spread function (PSF) image.

Figure 1 shows the deconvolved SZE image in contours overlaid on a color scale PSPC X-ray image of Abell 1835. The X-ray image is the PSPC "raw" counts image smoothed with a Gaussian with $\sigma = 15''$. The X-ray data contain roughly 5000 cluster counts with an image peak of 183 counts.

3 Method

3.1 Angular Diameter Distance Calculation

The calculation begins by constructing a model for the cluster gas distribution. We use a spherical isothermal β model to describe the ICM. Within this context the cluster's characteristic scale along the line of sight is the same as the scale in the plane of the sky. Cluster asphericities introduce an important uncertainty in the SZE and X-ray derived distance for a given cluster but should not result in any significant bias in the Hubble parameter derived from a large sample of clusters free from selection biases.[8]

The spherical isothermal β model is given by[9,10]

$$n_e(\mathbf{r}) = n_{e0}\left(1 + \frac{r^2}{r_c^2}\right)^{-3\beta/2}, \tag{1}$$

where n_e is the electron number density, r is the radius from the center of the cluster, r_c is the core radius of the ICM, and β is the power law index. With this model, the SZE signal is

$$\Delta T = f_{(x)} T_{\rm CMB} D_{\rm A} \int d\zeta \, \sigma_{\rm T} n_e \frac{k_{\rm B} T_e}{m_e c^2} = \Delta T_0 \left(1 + \frac{\theta^2}{\theta_c^2}\right)^{(1-3\beta)/2}, \tag{2}$$

where ΔT is the SZE decrement/increment, $f_{(x)} = (x\frac{e^x+1}{e^x-1} - 4)(1 + \delta_{\rm SZE})$ ($f_{(x)} \rightarrow -2$ in the non-relativistic and Rayleigh-Jeans limits) is the frequency dependence of the SZE with $x = h\nu/kT_{\rm CMB}$, $\delta_{\rm SZE}(x, T_e)$ is the relativistic correction to the frequency dependence, $T_{\rm CMB} = 2.728$ K is the temperature of the CMB radiation,[11] $k_{\rm B}$ is the Boltzmann constant, $\sigma_{\rm T}$ is the Thompson cross section, m_e is the mass of the electron, c is the speed of light, ΔT_0 is the central SZE decrement/increment, θ is the angular radius in the plane of the sky and θ_c the corresponding angular core radius, and the integration is along the line of sight $\ell = D_{\rm A}\zeta$. We apply the relativistic corrections $\delta_{\rm SZE}$ to fifth order in $kT_e/m_e c^2$ of Itoh et al.[12] The Itoh et al. results agree

with other work[13,14] to third order where they stop. This correction decreases the magnitude of $f_{(x)}$ by about 3% for most clusters in this sample. The correction increases (in magnitude) with increasing electron temperaure.

The X-ray surface brightness is

$$S_x = \frac{1}{4\pi(1+z)^4} D_{\rm A} \int d\zeta \, n_e n_{\rm H} \Lambda_{e{\rm H}} \; = S_{x0} \left(1 + \frac{\theta^2}{\theta_c^2}\right)^{(1-6\beta)/2}, \qquad (3)$$

where S_x is the X-ray surface brightness in cgs units (erg s^{-1} cm^{-2} arcmin^{-2}), z is the redshift of the cluster, $n_{\rm H}$ is the hydrogen number density of the ICM, $\Lambda_{e{\rm H}} = \Lambda_{e{\rm H}}(T_e, {\rm abundance})$ is the X-ray cooling function of the ICM in the cluster rest frame in cgs units (erg cm^3 s^{-1}) integrated over the redshifted *ROSAT* band, and S_{x0} is the X-ray surface brightness in cgs units at the center of the cluster. The normalizations, ΔT_0 and S_{x0}, used in the fit include all of the physical parameters and geometric terms that come from the integration of the β model along the line of sight.

One can solve for the angular diameter distance by eliminating n_{e0} (noting that $n_{\rm H} = n_e \mu_e / \mu_{\rm H}$ where $n_j \equiv \rho / \mu_j m_p$ for species j) yielding

$$D_{\rm A} = \frac{(\Delta T_0)^2}{S_{x0}} \left(\frac{m_e c^2}{k_{\rm B} T_{e0}}\right)^2 \frac{\Lambda_{e{\rm H}0} \mu_e / \mu_{\rm H}}{4\pi^{3/2} f_{(x)}^2 \, T_{\rm CMB}^2 \, \sigma_{\rm T}^2 \, (1+z)^4} \frac{1}{\theta_c} \left[\frac{\Gamma(\frac{3}{2}\beta)}{\Gamma(\frac{3}{2}\beta - \frac{1}{2})}\right]^2 \frac{\Gamma(3\beta - \frac{1}{2})}{\Gamma(3\beta)} \qquad (4)$$

for the spherical isothermal β model, where $\Gamma(x)$ is the Gamma function. Similarly, one can eliminate $D_{\rm A}$ instead and solve for the central density n_{e0}.

3.2 Joint SZE and X-ray Model Fitting

The SZE and X-ray emission both depend on the properties of the ICM, so a joint fit to all the available data provides the best constraints on those properties. We perform a maximum likelihood joint fit to the interferometric SZE data and the PSPC and HRI X-ray data. Each data set is assigned a collection of parametrized models. Typically, SZE data sets are assigned a β model and point sources and X-ray images are assigned a β model and a cosmic X-ray background model. This set of models is combined for each data set to create a composite model that is then compared to the data. The data sets are independent so the likelihoods for each data set can be multiplied together. Likelihoods are computed using Gaussian statistics for the interferometric SZE data and Poisson statistics for the X-ray data.

Unlike X-ray instruments, interferometers do not directly measure the sky intensity. Instead, interferometers measure the Fourier transform of the sky brightness distribution multiplied by the primary beam. The primary beam is a Gaussian-like attenuation on the sky from the finite aperature of each dish; it limits the field of view of the interferometer. Therefore, we fit to the interferometric data directly in the Fourier plane, where the spatial filtering and the noise characteristics of the interferometer are well understood. We construct the SZE model in the image plane, take the Fourier transform, and compare with the interferometric SZE data in the Fourier plane.

4 Results and Conclusion

We perform the maximum-likelihood joint fit to the SZE and X-ray data and compute the angular diameter distance to each of our 14 high redshift galaxy clusters. There is a known correlation between the β and θ_c parameters of the β model. One might think this correlation would make determinations of $D_{\rm A}$ imprecise because $D_{\rm A}$ is calculated from these very shape parameters of the ICM. Figure 2 illustrates this correlation and its effect on $D_{\rm A}$ for Cl 0016+16.

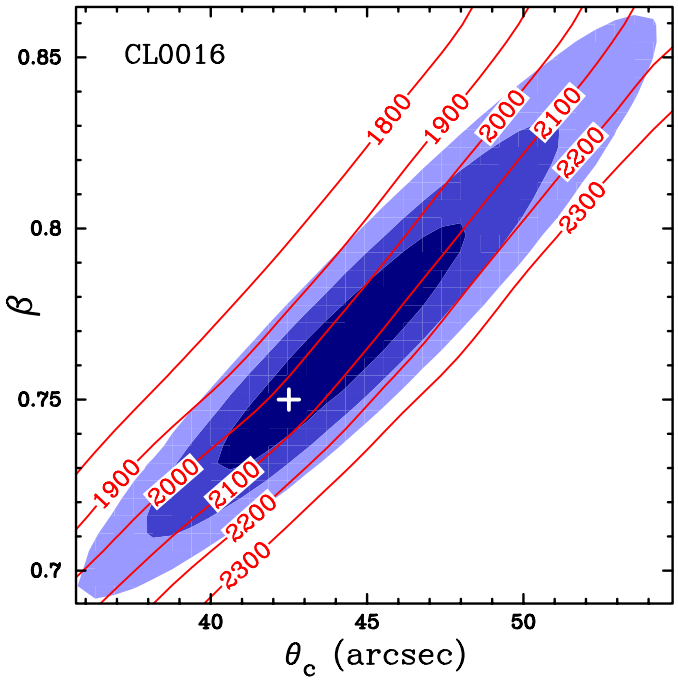

Figure 2: Confidence regions from the joint SZE and X-ray fits for Cl 0016+16. The filled regions are the 1,2, and 3 σ confidence regins for β and θ_c jointly, and the cross marks the best-fit β and θ_c. Solid lines are contours of angular diameter distance in megaparsecs. The $D_{\rm A}$ contours lie roughly parallel to the β-θ_c correlation, minimizing the effect of this correlation on the unertainties of $D_{\rm A}$.

The filled contours are the 1, 2, and 3 σ confidence regions for β and θ_c jointly. The lines are contours of constant $D_{\rm A}$ in Mpc. With our interferometric SZE data, the contours of constant $D_{\rm A}$ lie roughly parallel to the β-θ_c correlation, minimizing the effect of this correlation on the uncertainties of $D_{\rm A}$.

The SZE determined distances to our 14 high redshift clusters are shown in Figure 3 versus redshift. The error bars include the statistical uncertainty only. Theoretical angular diameter distance relations are plotted for three different cosmologies assuming $H_0 = 60$ km s^{-1} Mpc^{-1}. The distances follow the expected general trend versus redshift. Note that many of these distances are about 1000 Mpc, which is a sizeable fraction of the radius of the Hubble volume.

To determine the Hubble Constant, we perform a χ^2 fit to our calculated $D_{\rm A}$'s versus z for three different cosmologies. To estimate statistical uncertainties, we combine the uncertainties on $D_{\rm A}$, summarized in Table 1, in quadrature. This combined statistical uncertainty is symmetrized (averaged) and used in the fit. We find

$$H_0 = \begin{cases} 63^{+4\ +19}_{-4\ -19}\ \text{km s}^{-1}\ \text{Mpc}^{-1}; & \Omega_M{=}0.3,\ \Omega_\Lambda{=}0.7, \\ 59^{+4\ +18}_{-4\ -18}\ \text{km s}^{-1}\ \text{Mpc}^{-1}; & \Omega_M{=}0.3,\ \Omega_\Lambda{=}0.0, \\ 56^{+4\ +17}_{-4\ -17}\ \text{km s}^{-1}\ \text{Mpc}^{-1}; & \Omega_M{=}1.0,\ \Omega_\Lambda{=}0.0, \end{cases} \quad (5)$$

where the uncertainties are statistical followed by systematic at 68% confidence. The statistical error comes from the χ^2 analysis and includes uncertainties from T_e, the parameter fitting, metallicity, and $N_{\rm H}$ (see Table 1 for approximate percentage statistical uncertainties).

The systematic uncertainties have been added in quadrature and include an 8% (4% in ΔT_0) uncertainty from the absolute calibration of the SZE data, a 10% effective area uncertainty for the PSPC and HRI, a 5% uncertainty from the column density, a 5% ($\simeq 20/\sqrt{14}$) uncertainty due to asphericity, a 20% effect for our assumptions of isothermality and single-phase gas, a 16% (8% in ΔT_0) uncertainty from undetected radio sources, and a 2% ($\simeq 8/\sqrt{14}$) uncertainty from the kinetic SZE. These systematic uncertainties are summarized in Table 2. The contributions

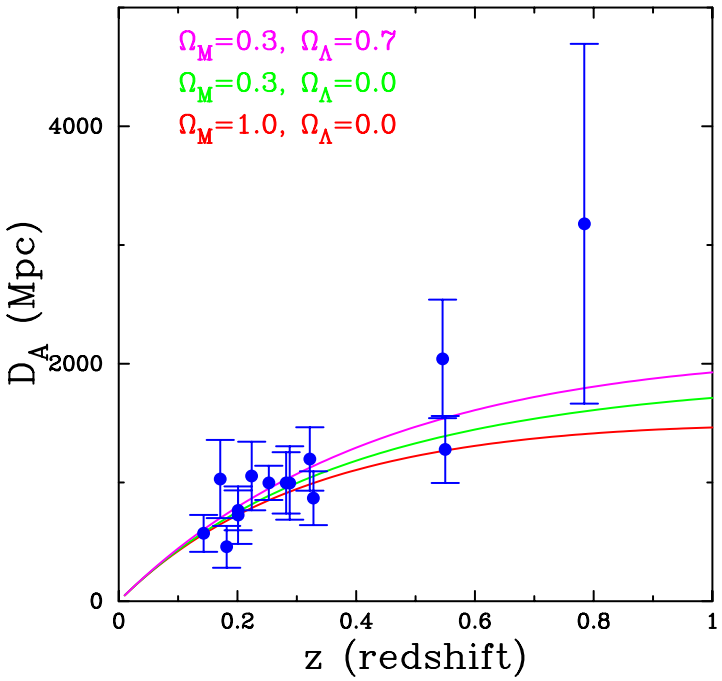

Figure 3: SZE determined angular diameter distances versus redshift for our 14 high redshift cluster sample. The error bars include statistical uncertainties only. The theoretical angular diameter distance relation is plotted for three different cosmologies, assuming $H_0 = 60$ km s^{-1} Mpc^{-1}.

from asphericity and kinetic SZE should average out for a large sample. Though daunting, these systematics are controllable. We briefly discuss the controllable nature of each of these possible sources of systematics.

Table 1: Approximate Statistical Uncertainties

Systematic	Effect (%)
T_e	± 20
Parameter fitting	± 15
metallicity	± 1
$N_{\rm H}$	± 1
Total[a]	± 25

[a] Combined in quadrature.

There is currently work being done to improve the absolute calibration of the 30 GHz interferometer with a goal of a 1% calibration. The current generation of X-ray satelites will greatly reduced the uncertainty from the X-ray calibration, bringing the 10% absolute calibration of ROSAT down to the few percent level. These satelites will also address the isothermality and cluster sub-structure issues. Radio point sources in the cluster field below our detection threshold will affect the distance to that cluster. We have proposed to observe our cluster fields with multi-wavelength observations at the VLA, which will reduce the undetected point source uncertainty to negligable levels. Finally, asphericity and kinetic SZE contamination will be controlled by using larger samples of clusters that are forthcoming from Chandra and XMM-Newton and from next generations SZE experiments.

We currently have 35 clusters with high signal to noise interferometric SZE data. Therefore we can increase the sample size, further reducing the effects of asphericity and contamination

Table 2: H_0 Systematic Uncertainty Budget

Systematic	Effect (%)
SZE calibration	± 8
X-ray calibration	± 10
$N_{\rm H}$	± 5
Asphericity[a]	± 5
Isothermality & clumping	± 20
Undetected radio sources	± 16
Kinetic SZE[a]	± 2
Total[b]	± 33

[a] Includes a $1/\sqrt{14}$ factor for our 14 cluster sample.
[b] Combined in quadrature.

from the kinetic SZE. Approximately 10 of these clusters have a redshift greater than 0.5, with the highest redshift cluster at $z \sim 0.9$. With the ever increasing sample of high redshift clusters, we will be able to constrain the geometry of the universe from the combined analysis of SZE and X-ray data, providing a check on the recent type Ia supernovae results.[15,16]

Acknowledgments

This work is supported by NASA LTSA grant NAG5-7986. EDR gratefully acknowledges support from NASA GSRP Fellowship NGT5-50173. We thank Gilbert Holder and John Hughes for enlightening discussions.

References

1. Sunyaev, R. & Zel'dovich, Y. 1970, Comments Astrophys. Space Phys., 2, 66
2. Sunyaev, R. A. & Zel'dovich, Y. B. 1972, Comments Astrophys. Space Phys., 4, 173
3. Reese, E. D. et al. 2000, ApJ, 533, 38
4. Carsltrom, J. E., Joy, M., and Grego, L. E. 1996, ApJ, 456, L75
5. Carsltrom, J. E., Joy, M. K., Grego, L., Holder, G. P., Holzapfel, W. L., Mohr, J. J., Patel, S., and Reese, E. D. 1999, Physical Scripta, in press, astroph/9905255.
6. Snowden, S. L., McCammon, D., Burrows, D. N., & Mendenhall, J. A. 1994, ApJ, 424, 714
7. Snowden, S. L. 1998, ApJS, 117, 233
8. Sulkanen, M. E. 1999, ApJ, 522, 59
9. Cavaliere, A. & Fusco-Femiano, R. 1976, Astronomy and Astrophysics, 49, 137
10. —. 1978, Astronomy and Astrophysics, 70, 677
11. Fixsen, D. J., Cheng, E. S., Gales, J. M., Mather, J. C., Shafer, R. A., & Wright, E. L. 1996, ApJ, 473, 576
12. Itoh, N., Kohyama, Y., & Nozawa, S. 1998, ApJ, 502, 7
13. Stebbins, A. 1997, preprint: astro-ph/9709065
14. Challinor, A. & Lasenby, A. 1998, ApJ, 499, 1
15. Schmidt, B. P., et al. 1998, ApJ, 507, 46
16. Perlmutter, S., et al. 1999, ApJ, 517, 565